A hierarchical model for surface effects on chain conformation and rheology of polymer solutions. II. Application to a neutral surface

Vlasis G. Mavrantzas[a] and Antony N. Beris[b]
Department of Chemical Engineering, University of Delaware, Newark, Delaware 19716

(Received 29 July 1998; accepted 23 September 1998)

In this part, the general formulation described in Part I is applied to the modeling of the behavior of a dilute polymer solution near a purely repulsive, planar solid surface, i.e., near a noninteracting wall. The static equilibrium problem is considered first. The model equations here reduce to a minimization problem for the Helmholtz free energy of the system, which results into the well known equilibrium condition that the chemical potentials of all chain conformations in the interfacial area should be equal to each other. The numerical results show that the loss of polymer conformational entropy in the interfacial region gives rise to a strong polymer depletion which extends up to a distance about three times the equilibrium root-mean-square polymer end-to-end distance. Next, the problem of a polymer solution flowing past the wall is investigated. Here, the full model equations need to be considered; these are solved numerically with a spectral collocation technique. The numerical results show that the flow field enhances polymer depletion phenomena near the wall relative to those observed under equilibrium (static) conditions: By increasing the shear stress, the polymer concentration in the interfacial area decreases, in full agreement with available experimental data. Moreover, the flow field is found to affect significantly the chain conformations near the wall: The applied shear stress is seen to extend the chains along a primary direction, ξ, and to depress them in the transverse direction, η. The depletion of the interfacial region in polymer molecules is further seen to lead to the formation of a boundary layer close to the wall, where the macroscopic fluid velocity increases rapidly from its zero value exactly at the wall to its asymptotic bulk profile, resulting into an apparent macroscopic slip at the wall. The theoretically calculated slip coefficient is found to be of the same order of magnitude with the experimentally measured one, as reported in the literature for a dilute polymer solution of polymethylacrylate flowing near a glass surface [H. Mueller-Moehnssen *et al.*, J. Rheol. **34**, 223 (1990)]. © *1999 American Institute of Physics.* [S0021-9606(99)50801-5]

I. INTRODUCTION

In Part I[1] we have addressed the problem of modeling the behavior of a polymer solution over a solid surface under both equilibrium (static) and nonequilibrium (flowing) conditions. The analysis was based on the Hamiltonian formulation of transport phenomena[2–9] in systems characterized by a complex internal microstructure in the framework of the generalized bracket formalism.[6] In particular, in Part I we showed how to systematically account for the presence of multiple length scales by deriving macroscopic equations which couple, through the use of selected internal field variables with the system microstructure. This hierarchical approach is shown to lead to a natural coupling of the macroscopic flow equations with the microscopic chain conformation, through the system Hamiltonian H. In particular, we showed that the velocity field and the chain concentration should vary in response, among other things, of generalized forces dictated by the nonequilibrium thermodynamics of the chain conformation. In return, the chain conformation changes in response to changes in the velocity and concentration field. The single, most important, quantity describing these macro–micro interactions is seen to be the generalized propagator G', accounting for the distribution function for the chain end-to-end vector under flow conditions, used in the definition of the system Hamiltonian.

The present approach presents a refinement of our previous work[10] on slip phenomena developed during the flow of polymer solutions near a noninteracting surface (a wall), where a Gaussian form had been assumed for the distribution function for the chain end-to-end distance vector everywhere in the flow domain, even at microscopic distances from the wall. Here, this assumption is removed, and instead, a self-consistent mean-field approach is followed, based on the random flight chain model, which allows us to describe consistently chain conformation changes near the wall due to the macroscopically imposed flow field. This also permits reducing the length scale of analysis of microscopic deformations from distances commensurate with the average end-to-end chain length (which is the minimum length scale for which the previously assumed Gaussian approximation was valid) down to distances commensurate with the length of the repeat (polymer segment) unit.

[a]Present address: Department of Chemical Engineering, University of Patras, and Institute of Chemical Engineering and High-Temperature Chemical Processes, Patras, Greece 26500.
[b]Author to whom correspondence should be addressed. Electronic mail: beris@che.udel.edu

The work is similar to the approach followed by Ploehn and Russel[11] in their study of the conformational properties of a polymer solution near a solid surface under equilibrium conditions through a continuum model. Although both the segment and the polymer chain density (and not only the segment volume fraction as was done in the Ploehn and Russel model[11]) are used in the present work in the expression for the extended free energy of the system, both approaches represent the same continuum description of the discrete lattice model of Scheutjens–Fleer,[12] and they naturally reduce to that in the limit of very long chains. As we will see, however, the present methodology is much more general and fundamental, and allows us to extend these previous works to flowing conditions as well.

As already mentioned above, the single, most important, quantity describing the coupling between macro–micro interactions in our approach is the propagator $G'(\mathbf{R}+\mathbf{r}_0, N-1; \mathbf{r}_0, \boldsymbol{\alpha})$, which shows how the distribution function for the N-bead long chain end-to-end vector $\mathbf{R}$ is altered due to the imposed flow field in the y direction, characterized by the apparent strain tensor $\boldsymbol{\alpha}$. To specify $G'(\mathbf{R}+\mathbf{r}_0, N-1; \mathbf{r}_0, \boldsymbol{\alpha})$, in Part I of the paper,[1] a microscopic model was invoked, whose equations define the statistics of chain conformations near the surface consistently with the imposed flow field through the concept of the apparent strain tensor $\boldsymbol{\alpha}$. The apparent strain tensor $\boldsymbol{\alpha}$ defines how the conformation $\mathbf{c}_0$ of a polymer molecule which has already been altered by the solid surface is augmented due to the flow field, through

$$\mathbf{c} = \boldsymbol{\alpha} \cdot \mathbf{c}_0 \cdot \boldsymbol{\alpha}^T. \tag{1}$$

The propagator $G'(\mathbf{R}+\mathbf{r}_0, N-1; \mathbf{r}_0, \boldsymbol{\alpha})$ defines the probability for a chain with its start at the point $\mathbf{r}_0=(x_0, y_0, z_0)$ above the boundary to have an end-to-end vector $\mathbf{R}$, given that the apparent strain tensor is $\boldsymbol{\alpha}$. With the use of $\boldsymbol{\alpha}$ and $G'(\mathbf{R}+\mathbf{r}_0, N-1; \mathbf{r}_0, \boldsymbol{\alpha})$, a complete, closed set of macroscopic–microscopic equations has been derived for the macroscopic quantities of interest, which can be solved numerically as a function of the imposed flow field. Such quantities include the polymer concentration, the overall polymer chain conformation, and the velocity profile in the flow domain near the solid boundary. The structure of the rest of this paper is as follows: In Sec. II, the governing equations are presented for a steady-state simple shear flow over a stationary, noninteracting solid surface. The solution for static equilibrium is presented in Sec. III, mainly for validation purposes but also for comparison with the general (under flow) case which is presented in Sec. IV. The concluding remarks and a discussion of the most significant points are presented in Sec. V.

II. MODEL EQUATIONS

The governing equations consist of the concentration equation, the momentum equation along the flow and the shear directions, x and y, respectively, and the three constitutive equations for the three unknown components of the conformation tensor c_{xx}, c_{yy}, and c_{xy}. To get the final form of these equations, it is always helpful to keep in mind two things: (a) That all variables, i.e., the chain-end number density $n_{1,e}$, the velocity $\mathbf{v}$, the pressure p, and the conformation tensor $\mathbf{c}$ vary only along one direction, the shear direction y perpendicular to the surface, and (b) that only one velocity component is nonzero, the component ν_x, which according to (a) varies only along the y direction, i.e., $\nu_x=\nu_x(y)$, so that the flow kinematics is

$$\begin{aligned} &\nu_x = \nu_x(y), \\ &\nu_y = 0, \\ &\nu_z = 0. \end{aligned} \tag{2}$$

Then the macroscopic governing equations, Eqs. (11)–(16) of Part I, become as follows: The concentration equation becomes

$$\nabla_y \Pi + \frac{\partial h_i}{\partial y} - \frac{d\sigma_{yy}}{dy} = 0, \tag{3}$$

where

$$\Pi \equiv n_{1,e} \frac{\delta H_i}{\delta n_{1,e}} + \mathbf{C}: \frac{\partial h_i}{\partial \mathbf{C}} - h_i \tag{4}$$

is the osmotic pressure,

$$\boldsymbol{\sigma} \equiv 2\mathbf{C} \cdot \frac{\partial h_i}{\partial \mathbf{C}} \tag{5}$$

is the stress tensor, and

$$\begin{aligned} \frac{h_i(y_0)}{\rho_0 k_B T} &= u_s - \varphi_s \chi_s \delta(y_0) + \frac{1}{2} n_{1,e}(y_0) \ln\left[\frac{n_{1,e}(y_0)}{2} \frac{N}{Z(N-1,y_0)}\right] \\ &\quad + (1-\varphi(y_0))\ln(1-\varphi(y_0)) + \chi\varphi(y_0)(1-\varphi(y_0)) \\ &\quad - \frac{1}{2} n_{1,e}(y_0) \int_0^\infty \frac{G(\mathbf{R}+\mathbf{r}_0, N-1; y_0)}{Z(N-1,y_0)} \\ &\quad \times \ln\left[\frac{G'(\mathbf{R}+\mathbf{r}_0, N-1; y_0, \boldsymbol{\alpha})}{Z'(N-1,y_0;\boldsymbol{\alpha})} \frac{Z(N-1,y_0)}{G(\mathbf{R}+\mathbf{r}_0, N-1; y_0)}\right] d^3\mathbf{R} \end{aligned} \tag{6}$$

is the internal part of the Helmholtz free energy density. As extensively discussed in Part I, $n_{1,e}(y)$ and $\varphi(y)$ are not independent quantities but are related to each other through the integral constraint

$$\varphi(y) = \sum_{n=0}^{N-1} \int_0^\infty \frac{1}{2} n_{1,e}(y_0) G'(y, n; y_0, \boldsymbol{\alpha}) \times \frac{Z'(N-1-n, y; \boldsymbol{\alpha})}{Z'(N-1, y_0;, \boldsymbol{\alpha})} dy_0. \tag{7}$$

In Eq. (6) ρ_0 is the (constant) segment and solvent molecule number density, k_B the Boltzmann's constant, T the temperature, u_s the adsorption energy of a solvent molecule in k_BT units, φ_s the polymer segment surface fraction representing the chain segments adsorbed to the surface (it is zero when no polymer adsorption takes place), χ_s the surface energy of adsorbed polymer molecules, $\delta(y)$ the Dirac delta function, and $Z'(N-1, y; \boldsymbol{\alpha})$ the partition function

$$Z'(n,y_0;\boldsymbol{\alpha}) \equiv \int_0^\infty G'(y,n;y_0,\boldsymbol{\alpha})dy. \tag{8}$$

Note that in Eq. (6) the nonprimed propagator and partition function refer to the static equilibrium values (i.e., when $\boldsymbol{\alpha}=\mathbf{1}$, the unit tensor) of the corresponding primed quantities. Also note that in the above and the following, whenever the symbols $\mathbf{r}$ and $\mathbf{r}_0$, or their equivalents y and y_0, present dummy variables, they are used interchangeably in the equations.

The x component of the momentum equation becomes

$$\sigma_{yx}+\eta_s\frac{du_x}{dy}=\text{const.}=\tau_{yx}, \tag{9}$$

where η_s is the solvent viscosity and τ_{yx} the imposed (constant) total shear stress.

The y component of the momentum equation becomes

$$\nabla_y\Pi+\frac{\partial h_i}{\partial y}-\frac{d\sigma_{yy}}{dy}+\frac{dp}{dy}=0. \tag{10}$$

The xx component of the constitutive equation becomes

$$c_{xx}\frac{\partial h_i}{\partial c_{xx}}+c_{xy}\frac{\partial h_i}{\partial c_{xy}}=\left(\lambda K\rho_0\frac{n_{1,e}}{2}\right)c_{xy}\frac{du_x}{dy}. \tag{11}$$

The xy component of the constitutive equation becomes

$$2\left[c_{xx}\frac{\partial h_i}{\partial c_{xy}}+c_{xy}\frac{\partial h_i}{\partial c_{yy}}\right]=\left(\lambda K\rho_0\frac{n_{1,e}}{2}\right)c_{yy}\frac{du_x}{dy}. \tag{12}$$

And the yy component of the constitutive equation becomes

$$c_{xy}\frac{\partial h_i}{\partial c_{xy}}+c_{yy}\frac{\partial h_i}{\partial c_{yy}}=0. \tag{13}$$

By subtracting Eq. (3) from Eq. (10) it is seen that the pressure p is constant in the flow field. In addition, one can readily see from the definition of the stress tensor, Eq. (5), that the left-hand-side of Eq. (13) is simply the stress component σ_{yy}; therefore, $\sigma_{yy}=0$, and this implies that only the components σ_{xx} and σ_{xy} of the stress tensor $\boldsymbol{\sigma}$ are nonzero; these are needed in calculating $\nabla_y\Pi$. Since, in addition, the part of the internal free energy which is related to flow deformation is a function of the conformation tensor $\mathbf{c}$ through its dependence on the apparent strain deformation tensor $\boldsymbol{\alpha}$ and not on $\mathbf{c}$ directly, the governing equations need first to be transformed from functions of $\mathbf{c}$ to functions of $\boldsymbol{\alpha}$. If all this is done consistently and the final results are nondimensionalized, the governing equations take the following dimensionless form:

—The momentum equation along the x direction becomes

$$\sigma_{yx}+\beta\frac{du_x}{dy}=\text{const.}=\tau_{yx}, \tag{14}$$

where β is the viscosity parameter defined as the ratio of the solvent contribution to the polymer contribution to the total viscosity in the bulk

$$\beta=\frac{\eta_s}{\rho_0\frac{n_{1,b}}{2}k_BT\lambda}=\frac{\eta_s}{\eta_{p,b}}, \tag{15}$$

where $\eta_{p,b}$ is the polymer contribution to the viscosity in the bulk (λ being the characteristic relaxation time of the polymer).

—The concentration equation becomes

$$\nabla_y\ln\left[\frac{n_{1,e}(y)}{Z(N-1,y)}\right]-\frac{\partial f_{\text{def}}}{\partial\mathbf{c}}:\nabla_y\mathbf{c}=0. \tag{16}$$

—The three equations for the (three) independent components of the apparent strain tensor become

$$c_{xx}\frac{\partial f_{\text{def}}}{\partial\boldsymbol{\alpha}}:\frac{\partial\boldsymbol{\alpha}}{\partial c_{xx}}+c_{xy}\frac{\partial f_{\text{def}}}{\partial\boldsymbol{\alpha}}:\frac{\partial\boldsymbol{\alpha}}{\partial c_{xy}}=c_{xy}\frac{du_x}{dy}, \tag{17}$$

$$2\left[c_{xx}\frac{\partial f_{\text{def}}}{\partial\boldsymbol{\alpha}}:\frac{\partial\boldsymbol{\alpha}}{\partial c_{xy}}+c_{xy}\frac{\partial f_{\text{def}}}{\partial\boldsymbol{\alpha}}:\frac{\partial\boldsymbol{\alpha}}{\partial c_{yy}}\right]=c_{yy}\frac{du_x}{dy}, \tag{18}$$

and

$$c_{xy}\frac{\partial f_{\text{def}}}{\partial\boldsymbol{\alpha}}:\frac{\partial\boldsymbol{\alpha}}{\partial c_{xy}}+c_{yy}\frac{\partial f_{\text{def}}}{\partial\boldsymbol{\alpha}}:\frac{\partial\boldsymbol{\alpha}}{\partial c_{yy}}=0, \tag{19}$$

where f_{def} is the density of the flow contribution h_{def} to the internal free energy density, defined as

$$f_{\text{def}}\equiv\frac{h_{\text{def}}}{n_{1,e}}. \tag{20}$$

Since the flow contribution to the internal free energy density is given by the last term in Eq. (6), i.e., in scaled units

$$h_{\text{def}}(y_0)=-n_{1,e}(y_0)\int_0^\infty\frac{G(\mathbf{R}+\mathbf{r}_0,N-1;y_0)}{Z(N-1,y_0)}\times\ln\left[\frac{G'(\mathbf{R}+\mathbf{r}_0,N-1;y_0,\boldsymbol{\alpha})}{Z'(N-1,y_0;\boldsymbol{\alpha})}\times\frac{Z(N-1,y_0)}{G(\mathbf{R}+\mathbf{r}_0,N-1;y_0)}\right]d^3\mathbf{R}, \tag{21}$$

we find that

$$f_{\text{def}}(y_0)=-\int_0^\infty\frac{G(\mathbf{R}+\mathbf{r}_0,N-1;y_0)}{Z(N-1,y_0)}\times\ln\left[\frac{G'(\mathbf{R}+\mathbf{r}_0,N-1;y_0,\boldsymbol{\alpha})}{Z'(N-1,y_0;\boldsymbol{\alpha})}\times\frac{Z(N-1,y_0)}{G(\mathbf{R}+\mathbf{r}_0,N-1;y_0)}\right]d^3\mathbf{R}, \tag{22}$$

($\mathbf{r}_0=(x_0,y_0,z_0)$ denotes the starting point of the chain) which shows that f_{def} is a function only of the tensor $\mathbf{c}$, or equivalently of $\boldsymbol{\alpha}$, but not of $n_{1,e}$. In the above and the following, the following scaling has been used and then overbars are dropped:

$$\overline{n_{1,e}}=\frac{n_{1,e}}{n_{1,b}},\quad \overline{c_{\alpha\beta}}=\frac{c_{\alpha\beta}}{\overline{\frac{k_BT}{k}}},\quad \overline{\frac{du_x}{dy}}=\lambda\,\frac{du_x}{dy},$$

$$\overline{y}=\frac{y}{\sqrt{\overline{\frac{k_BT}{k}}}},\quad \overline{G'}=G'\left(\frac{k_BT}{k}\right)^{3/2},\quad \overline{h_i}=\frac{h_i}{\rho_0\,\frac{n_{1,b}}{2}\,k_BT},$$

$$\overline{\sigma_{\alpha\beta}}=\frac{\sigma_{\alpha\beta}}{\rho_0\,\frac{n_{1,b}}{2}\,k_BT}. \tag{23}$$

According to this, distances are scaled with the root-mean-square equilibrium end-to-end distance in the bulk R_0, i.e.,

$$R_0=\sqrt{\frac{k_BT}{k}}, \tag{24}$$

and the stresses with the modulus of elasticity G_0 of the polymer solution in the bulk

$$G_0=\rho_0\,\frac{n_{1,b}}{2}\,k_BT. \tag{25}$$

With this scaling, the characteristic velocity for our system of equations is defined by the ratio of R_0 over λ:

$$\nu_0=\frac{R_0}{\lambda}. \tag{26}$$

With the exception of the concentration equation, Eq. (16), which is an ordinary differential equation, all other equations are algebraic. However, even the concentration equation can be cast in an algebraic form if we make the approximation that

$$\frac{df_{\rm def}}{dy}\approx\frac{\partial f_{\rm def}}{\partial\mathbf{c}}:\nabla_y\mathbf{c}. \tag{27}$$

The validity of this approximation was checked numerically *a posteriori*, and was found to introduce a numerical error always less than 1%. With this approximation, the concentration equation, Eq. (16), becomes

$$\nabla_y\left(\ln\left[\frac{n_{1,e}(y)}{Z(N-1,y)}\right]-f_{\rm def}(\mathbf{c}(y))\right)=0, \tag{28}$$

from which it is easily seen that

$$n_{1,e}(y)=Z(N-1,y)\exp[f_{\rm def}(\mathbf{c}(y))-f_{\rm def}\mathbf{c}(\infty)]. \tag{29}$$

In this way, the chain end concentration profile can be calculated separately after the momentum and constitutive equations have been solved for the velocity gradient and the components of the strain tensor $\boldsymbol{\alpha}$, respectively. As explained in Part I, in order to close the above system of equations, one needs to know $G'(\mathbf{R}+\mathbf{r}_0,N-1;y_0,\boldsymbol{\alpha})$, a task far from trivial, since, it depends both on the type of the imposed flow field and the specific interactions between polymer chains and surface. The next sections of this part will show how $G'(\mathbf{R}+\mathbf{r}_0,N-1;y_0,\boldsymbol{\alpha})$ can be calculated in the case of a polymer solution in contact with a neutral (purely repulsive) solid wall. Section III deals with the static equilibrium problem where the flow is identically zero, and Sec. IV deals with the nonequilibrium flow problem where a constant shear stress is applied on the solution.

III. STATIC EQUILIBRIUM PROFILES

When polymer chains are in contact with a noninteracting (impermeable) wall ($\chi_s=-\infty$), they experience a decrease of their entropy due to the loss of conformations which cannot survive the imposition of the hard boundary. The decrease of conformational entropy results in an increase of their free energy, therefore, molecules move away from the surface to the bulk. In the following sections, this depletion phenomenon will be investigated by solving the model equations developed in Sec. II to the case of a quiescent polymer solution above a solid wall. In this case, $\boldsymbol{\alpha}=\mathbf{I}$ (the unit tensor), and the propagator $G'(\mathbf{R}+\mathbf{r}_0,N-1;y_0,\boldsymbol{\alpha})$ becomes $G(\mathbf{R}+\mathbf{r}_0,N-1;y_0)$, i.e., it reduces to its static equilibrium form. To calculate $G(\mathbf{R}+\mathbf{r}_0,N-1;y_0)$, we solve the corresponding diffusion equation that G satisfies, Eq. (20) of Part I.

The description of polymer conformations through a diffusion equation dates back to the pioneering work of Chandrasekhar[13] on the problem of random flights. In its original formulation this problem is described as follows: A particle undergoes a sequence of random displacements $\Delta\mathbf{r}_1=\mathbf{r}_1-\mathbf{r}_0$, $\Delta\mathbf{r}_2,=\mathbf{r}_2-\mathbf{r}_1,\ldots$, $\Delta\mathbf{r}_{N-1}=\mathbf{r}_{N-1}-\mathbf{r}_{N-2}$, the magnitude and direction of each one of which is considered to be independent of all the preceding ones. The probability that the position after the ith displacement lies in the open sphere $|\mathbf{r}-\mathbf{r}_i|<d\mathbf{r}_i$ is determined by the same unknown distribution function assigned *a priori*. Then the following question is asked: What is the probability $Z^{-1}G(\mathbf{r},n;\mathbf{r}_0)d\mathbf{r}$ (where Z is a normalization factor) that after n displacements the coordinates of the random walker lie in the open sphere $|\mathbf{r}-\mathbf{r}_n|<d\mathbf{r}_n$? Under certain assumptions, this problem of random flights is isomorphic to that of polymer chain conformations. Of course, this case necessarily implies that the probabilities for each chain segment orientation are independent of each other. For certain applications this might be a poor assumption necessitating an extension of the original analysis which causes additional difficulties. In particular, substantial difficulties are encountered when excluded-volume effects need to be taken into account. In this case, the position and orientation of a link along the polymer chain depends on the position of not only just the previous one but also of all the others. This explains the quite extensive literature on the subject.[14]

According to Edwards,[14] one way to overcome the complexity introduced by excluded-volume effects is by approximating the effects of interactions of monomers along the chain by a self-consistent field. Thus, the conformation of a chain is treated as a random walk in the presence of a potential field the magnitude of which, in turn, depends on the random walk realizations. Using the proper normalization in order to build chain statistics, Edwards[14] proved that for dilute solutions $G(\mathbf{r},n;\mathbf{r}_0)$ is given as the solution to the following diffusion equation:

$$\frac{\partial G(\mathbf{r},n;\mathbf{r}_0)}{\partial n}=\frac{\ell^2}{6}\nabla^2 G(\mathbf{r},n;\mathbf{r}_0)-\upsilon\varphi(\mathbf{r})G(\mathbf{r},n;\mathbf{r}_0), \quad (30)$$

subject to the initial condition

$$at \;\; n=0, \quad G(\mathbf{r},0;\mathbf{r}_0)=\delta(\mathbf{r}-\mathbf{r}_0), \quad (31)$$

and boundary conditions dictated by the specification of the problem. In particular, for the problem of chain conformations realized in a semi-infinite medium confined by an impenetrable surface located at the $y=0$ plane, the following boundary conditions apply:

$$\begin{aligned} &at \;\; y=\infty, \quad G(\mathbf{r},n;\mathbf{r}_0)=0,\\ &at \;\; y=0, \quad G(\mathbf{r},n;\mathbf{r}_0)=0. \end{aligned} \quad (32)$$

In Eq. (30), ℓ is the chain segment length, υ the excluded-volume parameter, defined by

$$\upsilon=\int_0^\infty (1-e^{-U(r)/k_BT})d^3\mathbf{r}, \quad (33)$$

where U is the potential between two segments separated by a distance r, and $\varphi(\mathbf{r})$ the segment number fraction at spatial location $\mathbf{r}$.

Although excluded-volume effects can, in general, be addressed by our formalism, the assumption of a dilute polymer solution here allows us to neglect the potential term in the diffusion equation. This and the assumption of isotropicity in the other two directions in which G remains Gaussian, imply that

$$G(\mathbf{r},n;\mathbf{r}_0)=G_x(x,n;x_0)G_y(y,n;y_0)G_z(z,n;z_0), \quad (34)$$

where, in scaled units

$$G_x(x,n;x_0)=\frac{1}{\sqrt{2\pi c^0_{xx,n}}}\exp\left(-\frac{(x-x_0)^2}{2c^0_{xx,n}}\right) \quad (35)$$

and

$$G_z(y,n;y_0)=\frac{1}{\sqrt{2\pi c^0_{zz,n}}}\exp\left(-\frac{(z-z_0)^2}{2c^0_{zz,n}}\right), \quad (36)$$

with (also in scaled units)

$$c^0_{xx,n}=c^0_{zz,n}=\frac{n}{N-1}, \quad (37)$$

whereas G_y satisfies

$$\frac{\partial G_y}{\partial n}=\frac{\ell^2}{6}\frac{\partial^2 G_y}{\partial y^2}, \quad (38)$$

with initial and boundary conditions corresponding to Eqs. (31) and (32) above. A point to notice here is that, by considering Eq. (30), we have implicitly neglected end effects. This is also an important assumption, since, for a Rouse chain (for example) in a flow field, inner parts of chains are much more affected than chain ends.

The solution to the above diffusion problem can be found by the method of images[15]

$$G_y=\frac{1}{\sqrt{2\pi c^0_{yy,n}}}\left(\exp\left[-\frac{(y-y_0)^2}{2c^0_{yy,n}}\right]-\left[-\frac{(y+y_0)^2}{2c^0_{yy,n}}\right]\right), \quad (39)$$

where (again in scaled units)

$$c^0_{yy,n}=\frac{n}{N-1}, \quad (40)$$

i.e., $c^0_{yy,n}$ as well as $c^0_{xx,n}$ and $c^0_{zz,n}$ coincide with the corresponding component of the second moment of the distribution function for an n-segment long sub-chain in the bulk. In writing down Eqs. (39) and (40), we have tacitly assumed that the mean-square end-to-end distance of the polymer chain modelled as a random walk of $N-1$ steps should be mapped to the mean-square end-to-end distance of the same polymer chain imposed by the macroscopic model, that is, we have used that

$$\frac{(N-1)\ell^2}{3}\equiv\frac{k_BT}{K}. \quad (41)$$

The partition function $Z(n,y_0)$ is found by applying Eq. (8), the result being

$$Z(n,y_0)=\mathrm{erf}\left(\frac{y_0}{\sqrt{2c^0_{yy,n}}}\right). \quad (42)$$

Equilibrium profiles are then calculated by assuming a zero flow field in the governing equations: In particular, by substituting Eq. (42) for $Z(n,y_0)$ into Eq. (29) for the concentration of chain end points, and by keeping in mind that, due to absence of flow effects, $h_{\mathrm{def}}=f_{\mathrm{def}}=0$, we get the following result for the profile of chain end points:

$$\frac{n_{1,e}(y)}{n_{1,b}}=\mathrm{erf}\left(\frac{y}{\sqrt{2c^0_{yy,N-1}}}\right). \quad (43)$$

The same result can also be obtained directly from the initial form of the governing equations: If a flow field equal to zero is assumed, then the model equations boil down to the usual equilibrium condition

$$\frac{\delta H_i}{\delta n_{1,e}}=\left.\frac{\delta H_i}{\delta n_{1,e}}\right|_b, \quad (44)$$

which simply states that, at equilibrium, the chemical potential of every conformation should be constant everywhere in the domain (the subscript b in Eq. (44) refers to bulk conditions).[12] Indeed, by neglecting flow effects in the expression for the Volterra derivative $\delta H_i/\delta n_{1,e}$, Eq. (40) of Part I, and by substituting it back into Eq. (44), Eq. (43) reported above is obtained straightforwardly.

From the calculated ditribution of chain ends, the density profile of chain middle points can be found through Eq. (25) of Part I, while the segment fraction profile can be found from Eq. (7) above. In fact, a closed form expression can be found for $\varphi(y)$ by approximating the summation by a suitable integral for high chain lengths N; It is found that

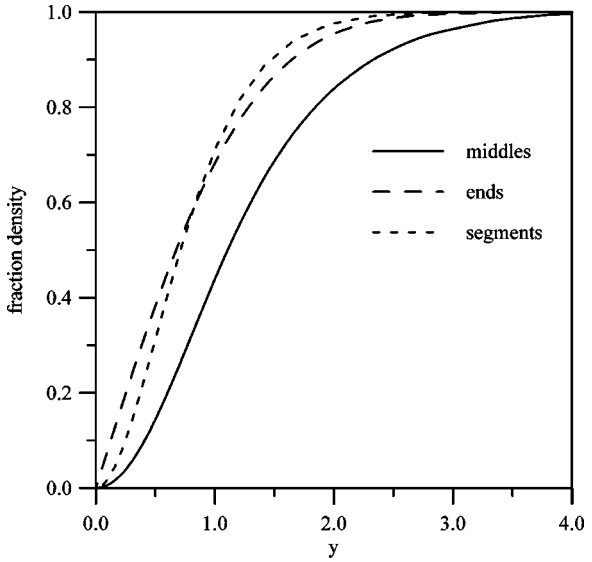

FIG. 1. The density of chain middle points $n_{1,m}$, chain end points $n_{1,e}$, and polymer segments φ as a function of the distance y from the wall scaled with the root-mean-square equilibrium end-to-end distance in the bulk R_0.

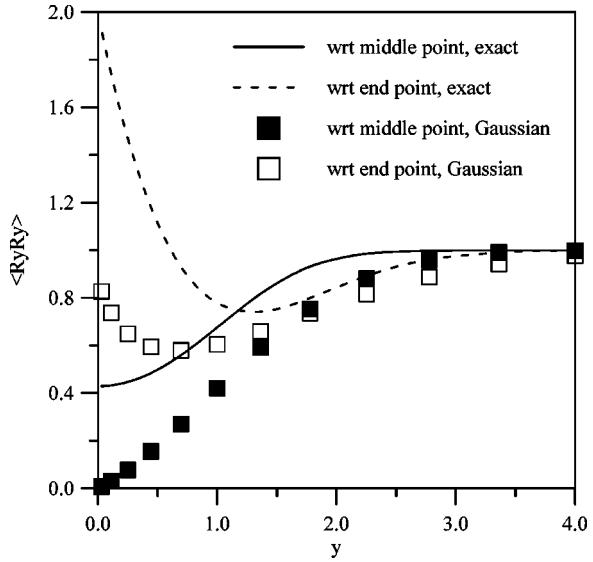

FIG. 2. The component $\langle R_y R_y \rangle$ of the second moment of the distribution function perpendicular to the wall as a function of the distance from the surface of the chain end point and the chain middle point obtained from the exact solution to the equations. The corresponding results obtained with the use of the Gaussian assumption are also indicated. In all cases, distances from the wall are scaled with the root-mean-square equilibrium end-to-end distance in the bulk R_0.

$$\frac{\varphi(y)}{\varphi_b} = 1 - 2\left(1 + \frac{y^2}{c^0_{yy,N-1}}\right)\mathrm{erfc}\left(\frac{y}{\sqrt{2c^0_{yy,N-1}}}\right) + \frac{2\sqrt{2}y}{\sqrt{\pi c^0_{yy,N-1}}}\exp\left(-\frac{y^2}{2c^0_{yy,N-1}}\right) + \left(1 + 4\frac{y^2}{c^0_{yy,N-1}}\right)\mathrm{erfc}\left(\frac{\sqrt{2}y}{\sqrt{c^0_{yy,N-1}}}\right) - \frac{2\sqrt{2}y}{\sqrt{\pi c^0_{yy,N-1}}}\exp\left(-\frac{2y}{\sqrt{c^0_{yy,N-1}}}\right), \tag{45}$$

which is in complete agreement with the findings of Ploehn and Russel[11] who did not consider chains in their analysis but probabilistically coupled $\varphi(y)$ to the partition function $Z(N-1,y)$.

The profiles of chain end points, chain middle points, and polymer segments are shown schematically in Fig. 1 where all quantities have been scaled with their bulk value. The horizontal axis denotes distance from the surface scaled with the equilibrium root-mean-square (rms) polymer end-to-end distance in the bulk R_0. According to this figure, starting from their bulk value, all $n_{1,e}$, $n_{1,m}$ and φ decrease monotonically as the solid surface is approached till they reach the value zero exactly on the surface. The length scale in all cases is the same, roughly three times R_0. However, the degree of depletion is different for the end points than for the middle ones: Indeed, although polymer segments and chain ends seem to suffer the same degree of depletion, chain middle points suffer a stronger depletion than chain end points. This happens because the conformational loss that a chain undergoes is much higher if its middle rather than its end point is brought closer to the surface: In the second case, chain conformations can still survive by developing perpendicularly to the wall.

This can be seen more clearly in Fig. 2 where the width of the distribution function in the direction perpendicular to the wall, $\langle R_y R_y \rangle$, is plotted as function of the distance from the wall of both the end, y_0, and the middle point, y_m, of the chain (both scaled with R_0). In the first case, $\langle R_y R_y \rangle$ shows an initial decrease as the chain starts to feel the confining effects of the solid wall until a minimum is attained, and then an increase takes place as the chain realizes more and more conformations perpendicularly to the wall. In contrast, when the middle point of the chain is brought close to the wall, $\langle R_y R_y \rangle$ exhibits a continuous decrease since conformations can develop only in the parallel direction. As a matter of fact, these trends had also been observed in the previous work,[10] where a Gaussian form (centered symbols in Fig. 2) had been assumed for the distorted from the wall distribution function (throughout this paper, we refer to that work as *the Gaussian approximation* due to the assumption of a Gaussian form with a variable width for the polymer end-to-end distribution function, as compared to *exact* for the present work, meaning that the *exact form* of the distribution function has been used in the calculations). However, the quantitative agreement with the results obtained using the exact distribution function is seen from the figure to be rather poor. For example, notice that, within the Gaussian assumption, $\langle R_y R_y \rangle$ is found to drop exactly to zero for a chain whose middle point is brought within an infinitesimal distance from the surface $(y_m \to 0)$. In contrast, the results with the exact distribution function show that $\langle R_y R_y \rangle$ reaches a finite value as y_m tends to zero.

IV. NONEQUILIBRIUM (FLOW) PROFILES

In this section, we want to evaluate the changes induced on the system by imposing a constant shear stress $\boldsymbol{\tau}_{yx}$ on it. To do so, we have to take two important steps. The first is to

calculate an exact solution for the propagator $G'(\mathbf{R}+\mathbf{r}_0, N-1; \mathbf{r}_0, \boldsymbol{\alpha})$ of the polymer molecules in the deformed state. The second is to substitute it into the model equations and solve them for the conformation tensor, the velocity field and the polymer concentration. To calculate G', we make the assumption that, in the deformed state, G' remains Gaussian in the neutral direction z, while in the plane of flow $(x-y)$, it obeys the deformed nonisotropic diffusion equation, Eq. (32) of Part I. That is, we make the assumption that

$$G'(\mathbf{r},n;\mathbf{r}_0,\boldsymbol{\alpha}) = G'_{\xi\eta}((\xi,\eta),n;(\xi_0,\eta_0),\boldsymbol{\alpha}) G'_z(z,n;z_0,\boldsymbol{\alpha}), \tag{46}$$

where

$$G'_z = \frac{1}{\sqrt{2\pi c^0_{zz,n}}} \exp\left(-\frac{(z-z_0)^2}{2c^0_{zz,n}}\right), \tag{47}$$

exactly as in the equilibrium case, whereas $G'_{\xi\eta}$ satisfies the following diffusion equation in the space of the eigenvector directions ξ and η of the tensor $\boldsymbol{\alpha}$:

$$\frac{\partial G'_{\xi\eta}}{\partial n} = D_1 \frac{\partial^2 G'_{\xi\eta}}{2\xi^2} + D_2 \frac{\partial^2 G'_{\xi\eta}}{\partial \eta^2}, \tag{48}$$

where n denotes the path length along the chain, and D_1 and D_2 are the two chain ''diffusivities'' driven by the strain tensor $\boldsymbol{\alpha}$ in the eigenvector directions ξ and η, respectively.

The transformation from the coordinate system (x,y) to eigenvector space (ξ,η) is given by

$$\begin{aligned} x &= \xi \cos\alpha - \eta \sin\alpha, \\ y &= \xi \sin\alpha + \eta \cos\alpha, \end{aligned} \tag{49}$$

where the angle a is defined as

$$\tan\alpha = \begin{cases} \dfrac{\sqrt{(b_{xx}-b_{yy})^2+4b_{xy}^2}-(b_{xx}-b_{yy})}{2b_{xy}}, & b_{xy}\neq 0 \\ 0, & b_{xy}=0 \end{cases}, \tag{50}$$

and the matrix $\mathbf{b}$ is given by

$$\mathbf{b} = \boldsymbol{\alpha}^2. \tag{51}$$

Based on Eq. (33) of Part I, the two diffusivities D_1 and D_2 in Eq. (48) are simply given (in dimensionless units) by

$$\begin{aligned} D_1 &= \frac{N-1}{2} b_{\xi\xi} \equiv \frac{N-1}{2} (a_{\xi\xi})^2, \\ D_2 &= \frac{N-1}{2} b_{\eta\eta} \equiv \frac{N-1}{2} (a_{\eta\eta})^2. \end{aligned} \tag{52}$$

Equation (48) needs to be solved together with the same initial and boundary conditions as for the equilibrium case, namely

$$\begin{aligned} &at\ \ t=0, \quad G' = \delta(x-x_0)\,\delta(y-y_0), \\ &at\ \ x=\pm\infty, \quad G'=0, \\ &at\ \ y=0, \quad G'=0, \\ &at\ \ y=+\infty, \quad G'=0, \end{aligned} \tag{53}$$

where $(x_0,y_0)=(0,y_0)$ is the location of chain origin and (x,y) the location of chain end in the (x,y) coordinate system.

To understand the physical meaning of Eq. (48) and its role in our formalism, we should notice the following two limiting cases: First, far away from any boundary conditions, the solution to Eq. (48) is a Gaussian function in the directions ξ and η with variances proportional to the corresponding second moments of the tensor $\mathbf{b}$, as dictated by the applied shear stress, i.e., for the full $(N-1)$-segment long chain

$$G'_{\xi\eta} = \frac{1}{\sqrt{(2\pi)^2 b_{\xi\xi} b_{\eta\eta}}} \exp\left(-\frac{(\xi-\xi_0)^2}{2b_{\xi\xi}} - \frac{(\eta-\eta_0)^2}{2b_{\eta\eta}}\right). \tag{54}$$

However, far away from the solid boundary, the equilibrium value of the macroscopic conformation tensor is the unit tensor, i.e., $\mathbf{c}_0 = \mathbf{1}$ (in scaled units); therefore, from Eq. (1), we find that, in the eigenvector space, the value of the macroscopic conformation tensor under the applied flow field is $\mathbf{c} = \boldsymbol{\alpha}\cdot\boldsymbol{\alpha}^T = \boldsymbol{\alpha}^2 = \mathbf{b}$ (in scaled units). By using this into Eq. (54) and substituting the result into Eq. (21) to calculate h_{def}, we obtain that

$$h_{\mathrm{def}} = \frac{n_{1,e}}{2}\left(\frac{1}{2}\,\mathrm{tr}(c) - \frac{1}{2}\,\ln\det(c)\right), \tag{55}$$

(in scaled units), which is exactly the one that produces the Maxwell model.[6,10] Second, in Sec. I, we saw that if flow effects are neglected and the two diffusivities in the x and y directions are those dictated by the Kuhn length ℓ, then Eq. (48) reduces to a one-dimensional (1D) diffusion equation, Eq. (38) above, in the y direction which very nicely reproduces the equilibrium profiles. Thus, the proposed equation, Eq. (48), constitutes a consistent generalization of the microscopic picture underlying the Maxwell model, in order to accommodate inhomogeneous, boundary-condition effects on chain conformations.

Flow effects in our work are, therefore, taken into account indirectly through the evaluation of the two diffusivities D_1 and D_2 that define the macromolecular conformation, thus, eliminating the necessity for the use of a potential function from the flow field. But the reader should immediately realize that this indirect accounting is done so as to always consistently satisfy the two important limits: First, it satisfies the equations in the bulk far away from any boundaries, and, second, it satisfies the equilibrium profiles near the boundary. In addition, the governing equations always satisfy the criterion of thermodynamic admissibility. In essence, our work here very much resembles the work of Treloar[16] who also used a strain parameter similar to tensor $\boldsymbol{\alpha}$ in order to define the variance of $\mathbf{c}$ in his work on rubber elasticity. The present work offers a consistent extension of his work to account for the resulting inhomogeneities due to boundary effects.

The solution to boundary-value problem, Eqs. (48)–(53), can be found again by the method of images and for the entire $(N-1)$-segment chain is given by

$$G'_{\xi\eta}=\frac{1}{2\pi\sqrt{b_{\xi\xi}b_{\eta\eta}}}\left[\exp\left(-\frac{(\xi-\xi_0)^2}{2b_{\xi\xi}}-\frac{(\eta-\eta_0)^2}{2b_{\eta\eta}}\right)-\exp\left(-\frac{(\xi-\xi_2)^2}{2b_{\xi\xi}}-\frac{(\eta-\eta_2)^2}{2b_{\eta\eta}}\right)\right], \tag{56}$$

where

$$\xi_2=\frac{(1-s^2)\xi_0+2s\eta_0\sqrt{\frac{D_1}{D_2}}}{1+s^2},$$

$$\eta_2=\frac{(s^2-1)\eta_0+2s\xi_0\sqrt{\frac{D_2}{D_1}}}{1+s^2}, \tag{57}$$

$$s=-\sqrt{\frac{D_1}{D_2}}\tan\alpha.$$

The partition function is next found from Eq. (8) as

$$Z'(y_0,\boldsymbol{\alpha})\equiv Z'(y_0,\mathbf{b})=\mathrm{erf}\left(\frac{y_0}{\sqrt{2b_{yy}}}\right), \tag{58}$$

see proof in Appendix B of Ref. 10.

The reader can now immediately see how the bulk limit, Eq. (55), can be recovered from Eq. (56): By letting the chain origin to lie at a distance y_0 far away from the solid boundary ($y_0\to\infty$), we have that

$$(\xi-\xi_2)^2\gg(\xi-\xi_0)^2,$$
$$(\eta-\eta_2)^2\gg(\eta-\eta_0)^2, \tag{59}$$

which means that the second term in Eq. (56) is unimportant; in addition, far away from the wall, $\mathbf{c}_0=\mathbf{I}$, and, as explained above, then $\mathbf{c}=\boldsymbol{\alpha}\cdot\boldsymbol{\alpha}^T=\boldsymbol{\alpha}^2=\mathbf{b}$. Using these equalities in Eq. (56) gives a Gaussian form for G', which, in three-dimensional (3D) space, identically reproduces the Maxwell model.

Having calculated G' and Z', the resulting model equations, Eqs. (17)–(22), (29), (56), and (58), can be solved numerically through a spectral collocation technique, and a zero-order continuation scheme in the shear stress τ_{yx} (starting from the equilibrium profiles), at a number of fixed points from the wall. In all cases, an exponential convergence was observed in the iteration scheme with the error tolerance criterion set up at 10^{-6}. Representative results for the profiles of the quantities of interest are shown in the next figures for various values of the imposed shear stress τ_{yx} and the viscosity parameter β. For comparison, in every figure, the results obtained with the use of the Gaussian approximation for the polymer end-to-end vector as reported in Ref. 10 are also shown.

In Figs. 3(a) and 3(b) we show typical profiles for the density of chain middle points for various imposed shear stress values τ_{yx} and two different values of the parameter β, 0.1 and 0.5, respectively. The use of such relatively small values may imply (depending on the molecular parameters used) strong chain overlaps, which could violate the dilute polymer solution assumption. These values were simply chosen in order to enable to comparison with available experimental data. The figures clearly show that the application of the shear stress shifts the equilibrium profiles to the right, i.e., it enhances the depletion phenomena in the interfacial region. Interestingly enough, this picture is the opposite of that observed with the use of the Gaussian approximation (upper group of curves in Fig. 3). Indeed, within the Gaussian approximation, the flow-induced shear stress is found to force the chains closer to the wall; furthermore, the quantitative agreement is quite poor. Notice though that in both groups of profiles, a limiting curve is reached for high enough values of τ_{yx}, beyond which τ_{yx} has no effect on the density profile. In addition, the profiles seem to be quite insensitive to the viscosity parameter β.

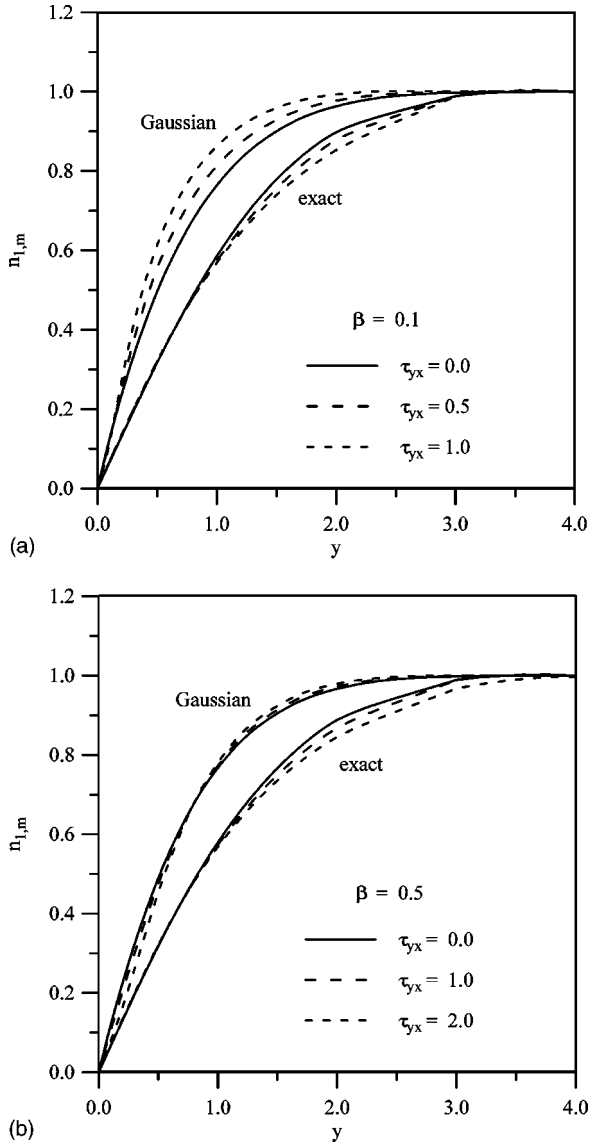

FIG. 3. The density of chain middle points $n_{1,m}$ as a function of the distance y from the wall for various shear stresses τ_{yx} and for two values of the viscosity parameter β, $\beta=0.1$ (a) and $\beta=0.5$ (b), respectively. The distance y is scaled with the root-mean-square equilibrium end-to-end distance in the bulk R_0. The upper set of curves corresponds to the ''fully Gaussian approximation'' whereas the lower set to the ''exact'' form for the distribution function near the wall.

Experimentally, polymer depletion phenomena near a wall have been studied by Ausserré *et al.*[17] through the

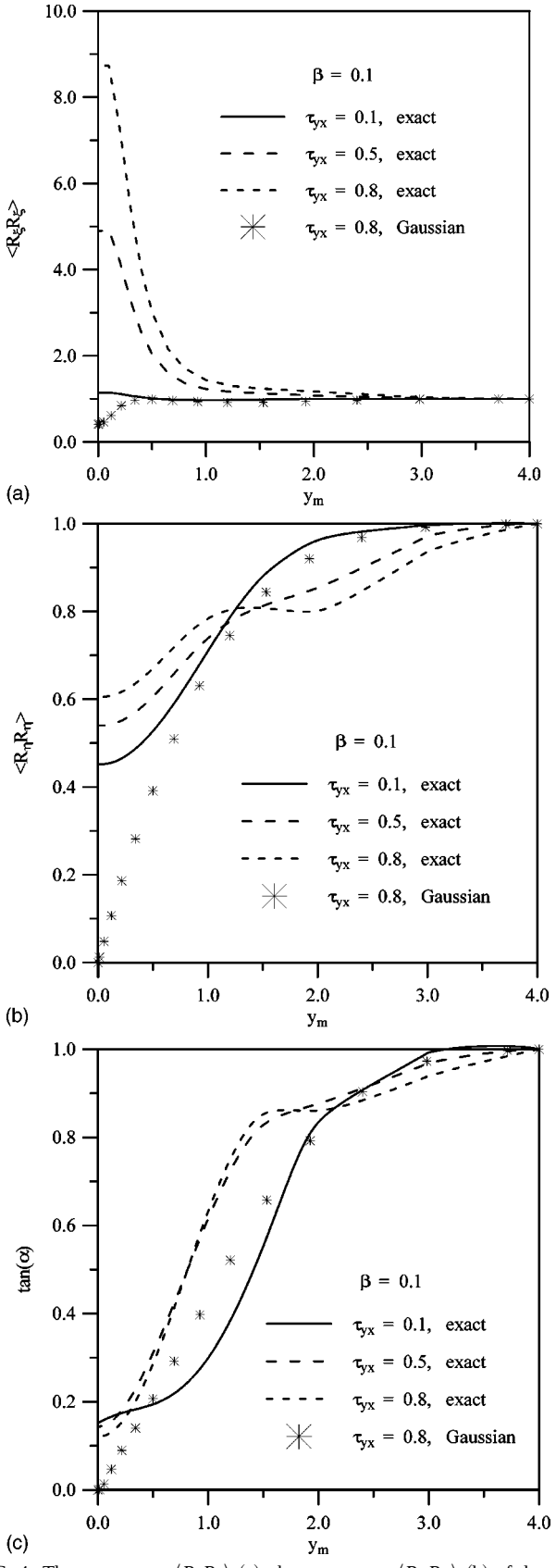

FIG. 4. The component $\langle R_\xi R_\xi \rangle$ (a), the component $\langle R_\eta R_\eta \rangle$ (b) of the second moment of the distribution function perpendicular to the wall, and the $\tan(\alpha)$ (c), as a function of the distance from the surface of the middle point of the chain for various shear stresses τ_{yx}. For the highest value of the shear stress ($\tau_{yx}=0.80$), the corresponding results obtained with the use of the Gaussian assumption are also indicated. Also $\beta=0.1$. In all cases, distances from the wall are scaled with the root-mean-square equilibrium end-to-end distance in the bulk R_0.

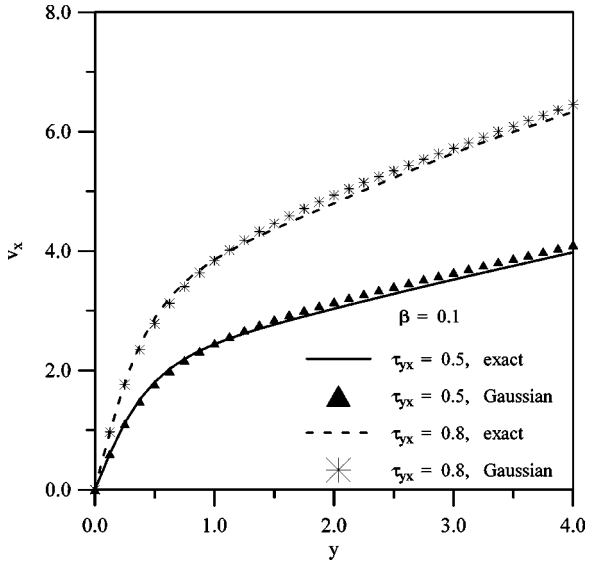

FIG. 5. The velocity ν_x as a function of the distance y from the wall for various shear stresses τ_{yx} and for $\beta=0.1$. The corresponding results obtained with the use of the Gaussian assumption are also indicated in centered symbols. The velocity is scaled with R_0/λ, where λ is the relaxation time of the polymer, and the distance with R_0.

evanescent-wave-induced-fluorescence technique (EWIF). For a dilute aqueous xanthan (a semirigid polysaccharide) solution above a nonadsorbing silica surface, they found that the shear rate increases the surface excess, which measures the extent of depletion, relative to that exhibited under equilibrium conditions. On the contrary, the Brownian dynamics simulations of Duering and Rabin[18] showed the depletion phenomena near the wall to decrease with the shear rate, which agreed with our earlier results based on the assumption of a Gaussian distribution function for the polymer statistics near the wall. The present work shows that if the exact distribution function is employed, then the theoretical findings are in agreement with the experimental observations.

In Figs. 4(a)–4(c) we show representative results for the effect of the shear stress on the conformational characteristics of the polymer chains. As such, we have chosen the two second moments of the distribution function in the eigenvector space, $\langle R_\xi R_\xi \rangle$ and $\langle R_\eta R_\eta \rangle$, respectively, and the angle of orientation α. In Fig. 4(a) in particular, we see that, as τ_{yx} increases, $\langle R_\xi R_\xi \rangle$ increases fast and monotonically. Indeed, for a viscosity ratio $\beta=0.1$ and a shear stress value $\tau_{yx}=0.8$, the chains near the wall are seen to be elongated by about 2 to 3 times than in the bulk of the flow. In contrast to the rapid increase of $\langle R_\xi R_\xi \rangle$, Figs. 4(b) and 4(c) show that the shear stress has a less dramatic effect on the other component $\langle R_\eta R_\eta \rangle$ and on the angle of orientation α. In all of these figures, the centered symbols denote the predictions of the Gaussian approximation.

The next figure, Fig. 5, is very important because it shows the velocity profile $\nu_x(y)$ in the interfacial region. As can be seen in this figure, ν_x, starting from the value zero on the wall, increases quite rapidly in the interfacial region before it reaches bulk characteristics, within a distance from the wall about two times the bulk rms end-to-end distance R_0. In the same figure, the results of the Gaussian approximation

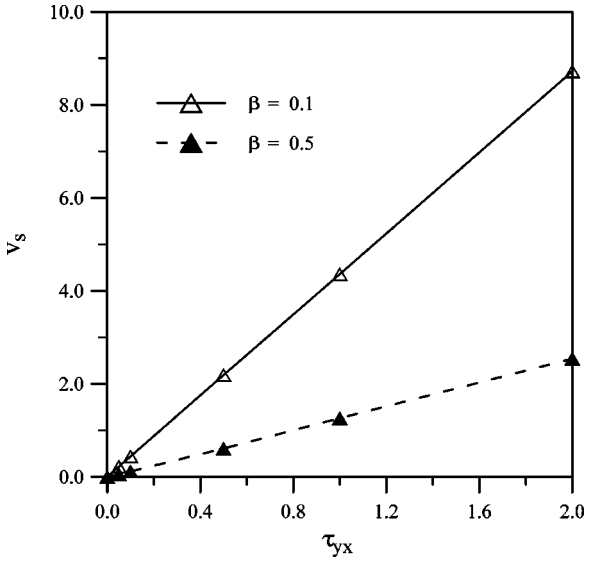

FIG. 6. The slip velocity ν_s as a function of the shear stresses τ_{yx} for two values of the viscosity parameter β, $\beta=0.1$ and $\beta=0.5$, respectively. The velocity is scaled with R_0/λ and the shear stress with the modulus of elasticity of the solution $G_0=\eta_{p,b}/\lambda$, where $\eta_{p,b}$ is the polymer viscosity in the bulk and λ the relaxation time of the polymer.

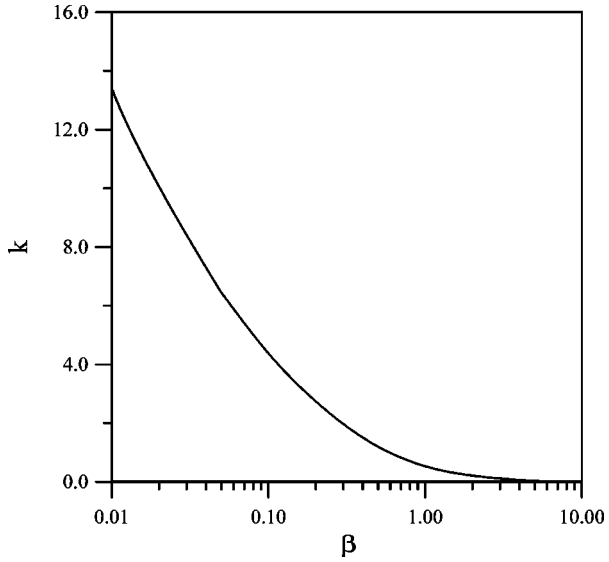

FIG. 7. The dimensionless slip coefficient k as a function of the viscosity parameter β. The slip coefficient is scaled with $R_0/\eta_{p,b}$.

are also represented by the centered symbols: In this case, the qualitative and quantitative agreement of the two approaches is excellent indeed. This happens because the velocity profile is a secondary rather than a primary quantity in our formalism: It is calculated through a simple integration after the velocity gradient, which is the quantity that explicitly enters into the governing equations, has been determined. The agreement is even more striking considering the qualitative and quantitative discrepancy of the Gaussian approximation for the concentration and conformational profiles. By further extrapolating the bulk velocity profile to intersect the wall, an apparent slip velocity ν_s can be defined which can be used to quantify the corresponding hydrodynamic boundary layer near the wall. According to Fig. 5, ν_s should be a strong function of the viscosity ratio parameter β and the imposed shear stress τ_{yx}. In the next figure, Fig. 6, we see that the slip velocity is practically a linear function of the shear stress τ_{yx}, thus, the ratio of the slip velocity over the shear stress, i.e., the (dimensionless) slip coefficient k, should be a function of only the viscosity ratio parameter β. Figure 7 shows exactly this dependence: As β increases, k decreases fast, and for $\beta>1.0$, k is essentially zero. In fact, according to scaling used above, it turns out that the slip velocity scales with R_0/λ so that the dimensional slip coefficient is a function not only of R_0 and β but also of the polymer viscosity $\eta_{p,b}$.

The linear dependence of the slip velocity on the shear stress has been verified experimentally by Mueller–Moehnssen *et al.*[19] in ducted flows of an electrolyte-free, aqueous solution of a high-molecular-weight, anionic polyacrylamide. Using a laser-differential anemometer and a total-reflection-microscope anemometer, these investigators were able to measure the velocity profile up to distances of 0.15 μm from the wall for a variety of polymer concentrations. For the lowest concentration (0.005% wt.), the measurements showed a sharp transition in the velocity profile at very small distances from the wall (on the order of the radius of gyration of the polymer chains, 0.1 μm) from zero to a finite value. This is the first instance where the apparent character of the slip phenomena has directly been verified experimentally. Quantitative comparison of their results with our model predictions, however, is not feasible at the present time, because additional electrostatic interactions between the charged PMA molecules and an electric double layer at the wall existed in the experiments for which the present model cannot account. A rough comparison has nevertheless been attempted where the parameters (data) entering into our model have been taken from the experimental work of Mueller-Moehnssen *et al.*[19] For the lowest polymer concentration (0.005% wt.) examined in the experiments, the experimentally measured slip coefficient k was found to be 4×10^{-3} cm^3/dyn/s whereas the model prediction is $(0.8\pm0.1)\times10^{-3}$ cm^3/dyn/s. It is seen, therefore, that by simply accounting for conformational changes near the wall, is enough to capture the correct order of magnitude of the slip phenomena. Moreover, the model prediction is lower than the experimentally measured value, which is quite pleasing, because the additional electrostatic repulsions for which the model cannot presently account are expected to enhance the depletion and slip phenomena in the interfacial area. For a more detailed comparison of our results for the velocity field with other experimental and available theoretical data in flows through membranes,[20–22] due to the consistency of the Gaussian approximation and the exact distribution function used in this paper regarding $\nu_x(y)$ and ν_x, we refer the interested reader to our previous publication.[10]

V. CONCLUSIONS

The major result of this work is that the shear stress is found to enhance the depletion phenomena near the wall, which is in contrast to the previous findings, based on the Gaussian assumption, that the shear stress drives the polymer

chains closer to the wall.[10] Indeed, the shear stress is found to shift the equilibrium profile for the density of chain middle points to the right which means that it drives chains further away from the surface. A second prediction of the new, more detailed work is that the component $\langle R_y R_y \rangle$ of the second moment of the distribution function perpendicular to the wall does not drop to zero exactly on the surface but reaches a finite, nonzero value there; on the contrary, the assumption of a Gaussian distribution function within the one-fluid model had resulted into a zero value of $\langle R_y R_y \rangle$ on the surface. As regards the velocity profile, however, the results of this and the previous work were found to be in very close agreement. In both models, the development of a boundary layer is seen to develop near the wall where the fluid velocity increases rapidly, thus, giving rise to an apparent slip velocity. Calculated slip velocities were found to depend linearly on the wall shear stress, corresponding, however, to different proportionality (slip) coefficients.

This paper has focused on the depletion phenomena near a wall which offers no attraction to polymer segments. Naturally, the question arises of how to extend the theory to account for attractive forces on polymer segments from an adsorbing surface. This issue of the combined surface adsorption–flow interaction has been an outstanding problem in polymer fluid dynamics, mainly because of its great technological interest due to the extended use of polymers as stabilizers in many applications. A forthcoming paper will address exactly this problem, and will further attempt to include into the analysis the effects of a solvent shear flow on the adsorbed polymer layer.

ACKNOWLEDGMENTS

We would like to acknowledge the financial support provided by NSF, Division of Fluid Mechanics and Hydraulics, Grant No. CTS-9114508. We would also like to thank Costas Dimitropoulos for his help in the preparation of the final manuscript.

[1] V. G. Mavrantzas and A. N. Beris, J. Chem. Phys. **110**, 616 (1999), preceding paper.
[2] J. P. Morrison, Phys. Lett. **100A**, 423 (1984).
[3] M. Grmela, Phys. Lett. **102A**, 355 (1984).
[4] M. Grmela, Phys. Lett. **130A**, 81 (1988).
[5] A. N. Beris and B. J. Edwards, J. Rheol. **34**, 503 (1990).
[6] A. N. Beris and B. J. Edwards *Thermodynamics of Flowing Systems* (Oxford University Press, New York, 1994).
[7] M. Grmela and H. C. Öttinger, Phys. Rev. E **56**, 6620 (1997).
[8] H. C. Öttinger and M. Grmela, Phys. Rev. E **56**, 6633 (1997).
[9] B. J. Edwards, A. N. Beris, and H. C. Öttinger, J. Non-Equil. Thermodynamics (in press).
[10] V. G. Mavrantzas and A. N. Beris, J. Rheol. **36**, 175 (1992).
[11] H. J. Ploehn, W. B. Russel, and C. M. Hall, Macromolecules **21**, 1075 (1988); H. J. Ploehn and W. B. Russel, *ibid.* **22**, 266 (1989).
[12] J. M. H. M. Scheutjens and G. J. Fleer, J. Phys. Chem. **83**, 1619 (1979).
[13] S. Chandrasekhar, Rev. Mod. Phys. **15**, 1 (1943).
[14] S. F. Edwards, Proc. Phys. Soc. Jpn. **85**, 613 (1965).
[15] W. Feller, *An Introduction to Probability Theory and its Applications* (Wiley, New York, 1966).
[16] L. R. G. Treloar *The Physics of Rubber Elasticity*, 3rd ed. (Oxford University Press, London, 1975).
[17] D. Ausserré, J. Edwards, J. Lecourtier, H. Hervet, and F. Rondelez, Europhys. Lett. **14**, 33 (1991).
[18] E. Duering and Y. Rabin, Macromolecules **23**, 2232 (1990).
[19] H. Mueller-Moehnssen, D. Weiss, and A. Tippe, J. Rheol. **34**, 223 (1990).
[20] G. Chauveteau, J. Rheol. **26**, 111 (1982).
[21] A. Omari, M. Moan, and G. Chauveteau, J. Rheol. **33**, 1 (1989).
[22] A. Omari, M. Moan, and G. Chauveteau, Rheol. Acta **28**, 520 (1989).